Research Article

Cancer Prevention Research

Nano-Bio-Chip Sensor Platform for Examination of Oral Exfoliative Cytology

Shannon E. Weigum[1], Pierre N. Floriano[1], Spencer W. Redding[4], Chih-Ko Yeh[4], Stephen D. Westbrook[4], H. Stan McGuff[5], Alan Lin[4], Frank R. Miller[6], Fred Villarreal[6], Stephanie D. Rowan[6], Nadarajah Vigneswaran[2], Michelle D. Williams[3], and John T. McDevitt[1]

Abstract

Oral cancer is a deadly and disfiguring disease that could greatly benefit from new diagnostic approaches enabling early detection. In this pilot study, we describe a nano-bio-chip (NBC) sensor technique for analysis of oral cancer biomarkers in exfoliative cytology specimens, targeting both biochemical and morphologic changes associated with early oral tumorigenesis. Here, oral lesions from 41 dental patients, along with normal epithelium from 11 healthy volunteers, were sampled using a noninvasive brush biopsy technique. Specimens were enriched, immunolabeled, and imaged in the NBC sensor according to previously established assays for the epidermal growth factor receptor (EGFR) biomarker and cytomorphometry. A total of 51 measurement parameters were extracted using custom image analysis macros, including EGFR labeling intensity, cell and nuclear size, and the nuclear-to-cytoplasmic ratio. Four key parameters were significantly elevated in both dysplastic and malignant lesions relative to healthy oral epithelium, including the nuclear area and diameter ($P < 0.0001$), the nuclear-to-cytoplasmic ratio ($P < 0.0001$), and EGFR biomarker expression ($P < 0.03$). Further examination using logistic regression and receiver operating characteristic curve analyses identified morphologic features as the best predictors of disease (area under the curve ≤0.93) individually, whereas a combination of all features further enhanced discrimination of oral cancer and precancerous conditions (area under the curve, 0.94) with high sensitivity and specificity. Further clinical trials are necessary to validate the regression model and evaluate other potential biomarkers, but this pilot study supports the NBC sensor technique as a promising new diagnostic tool for early detection of oral cancer, which could enhance patient care and survival.

Cancer Prev Res; 3(4); 518–28.

Introduction

Oral cancer, largely oral squamous cell carcinoma (OSCC), is a global health problem afflicting more than 300,000 people each year (1). In the United States alone, more than 35,000 new cases and nearly 8,000 deaths are estimated in 2008, representing approximately 3% of all cancers in men and 2% in women (2). Despite significant advances in surgical procedures and treatment, the long-term prognosis for patients with OSCC remains poor, with a 5-year survival rate of approximately 50%, which is among the lowest for all major cancers (2–4). This high mortality rate is often attributed to the advanced disease stage of many OSCCs on initial identification and biopsy. In contrast, if detected early, the prognosis for oral cancer patients is excellent with 5-year survival rates up to 90% (2, 4). In addition, management of early-stage oral cancer is often accomplished with less aggressive methods that can preserve vital organ function and physical appearance, resulting in a better quality of life for patients (3). This trend underscores the need for new diagnostic techniques targeting early tumor progression and molecular transformation, which could enable early detection of oral cancer.

The disease OSCC happens to be well suited for development of early detection and screening strategies due to the inherent accessibility of the oral cavity and the presence of premalignant lesions, which often precede the emergence of invasive OSCC. These lesions typically present clinically as leukoplakia (white lesions) and occasionally as erythroplakia (red lesions); however, only about 5% of these lesions will actually progress to cancer (5–7). Although some clinical signs, such as a nonhomogeneous surface or a stippled appearance, suggest a higher risk of malignant transformation, there are currently no reliable indicators of which lesions will progress (8). Standard good clinical practice dictates that all suspicious

Authors' Affiliations: [1]Departments of Chemistry and Bioengineering, Rice University; [2]Department of Diagnostic Science, University of Texas Health Science Center at Houston; [3]Department of Pathology, M.D. Anderson Cancer Center, Houston, Texas; and Departments of [4]Dental Diagnostic Science, [5]Pathology, and [6]Otolaryngology, Head and Neck Surgery, University of Texas Health Science Center at San Antonio, San Antonio, Texas

Corresponding Author: John T. McDevitt, Departments of Chemistry and Bioengineering, Rice University, 6100 Main St., Houston, TX 77005. Phone: 713-348-2123; Fax: 713-348-2081; E-mail: mcdevitt@rice.edu.

doi: 10.1158/1940-6207.CAPR-09-0139

lesions should be subjected to surgical biopsy and pathologic evaluation because histologic evidence of epithelial dysplasia is regarded as the most reliable indicator of malignant potential (8, 9). However, there are several major limitations of this approach. For one, the low rate of cancerous progression suggests that up to 95% of patients may receive an invasive diagnostic procedure unnecessarily, with associated cost, psychological effects, and physical morbidity. Furthermore, the grading of oral epithelial dysplasia (mild/moderate/severe) is subjective and notoriously unreliable with considerable inter- and intra-examiner variation in the histopathologic diagnosis (10, 11).

The use of exfoliative cytology offers a rapid, noninvasive method to obtain a sampling of epithelial cells from premalignant lesions, which may be subjected to microscopic or molecular examination for signs of malignant change. Yet, unlike cervical cancer screening that has used epithelial brushings or scrapings for decades, conventional oral cytology has long been viewed unfavorably with limited diagnostic ability and low sensitivity. These shortcomings have frequently been attributed to poor or inadequate cell sampling and subjectivity associated with cytologic interpretation and diagnosis (12). Recent improvements in specimen collection and quantitative image analysis techniques, including cytomorphometry and DNA aneuploidy, have stimulated a renewed interest in cytology for detection of oral malignancies (13, 14). In addition, exfoliative cytology has also emerged as an excellent, noninvasive method to obtain cellular material for DNA-, RNA-, and protein-based analysis of tumor biomarkers, shifting the clinical effect of oral cytology toward molecular diagnostic techniques (14–18). Bringing these two approaches together on a single nano-bio-chip (NBC) platform for molecular and morphologic analysis in oral exfoliative cytology may further enhance the role and utility of oral cytology in clinical diagnostics.

Currently, the only commercially available diagnostic adjunct using exfoliative cytology is the OralCDx Brush Test with computer-assisted analysis from OralScan Laboratories. In a large multicenter study, the OralCDx test showed high sensitivity and specificity (100% and 93%, respectively) for detection of atypical oral epithelia based on morphology, keratinization, and ploidy patterns (19). Unfortunately, in this study, scalpel biopsy was not done for all, or even the majority, of OralCDx "negative" or "atypical" specimens, possibly resulting in overestimation of the sensitivity/specificity for this test (19, 20). Despite promising results of the OralCDx test and initial interest in this new technique, concerns have arisen about the accuracy of this test due to high rates of false-positive test results. This is supported by Poate et al. (21) reporting a 71% sensitivity and a 32% specificity using the OralCDx system. Here, the low specificity may be due to flaws in the retrospective study design or the high occurrence of false-positive results associated with benign inflammatory conditions, such as lichen planus (19, 22). The latter suggests the need for additional disease-specific biomarkers, which may be used in conjunction with brush cytology, to improve molecular-level characterization of oral lesions (21, 22).

The cytoanalysis solution presented here based on the NBC synergizes components and achievements from nanotechnology, molecular diagnostic biomarker discovery, and microfluidics to create a powerful new measurement approach condensing all working components into a small device footprint. The NBC boasts of an extremely flexible assay design and has a diverse group of validated analyte subtypes, including nucleic acids, proteins, cells, and bacteria (23–26). Previously, we established the biochip sensor system for rapid detection and quantitation of the epidermal growth factor receptor (EGFR) biomarker in OSCC cell lines (27). The EGFR is a well-characterized biomarker associated with early oral tumorigenesis and aggressive cancer phenotypes that is overexpressed in up to 90% of all OSCCs (28, 29). In the current study, the integration of the NBC sensor system for concurrent and quantitative analysis of cellular biomarkers, using EGFR as an example, and cytomorphology is shown as a new technique for multifunctional cytoanalysis. In addition, this NBC sensor and methodology is tested in a clinical pilot group to secure an initial understanding of the diagnostic utility of such biosensor systems in clinical settings.

Materials and Methods

Sensor design and instrumentation

The design and fabrication of the membrane-based NBC platform has been described previously (27). Briefly, the cell-based NBC microfluidic sensor is a multilayered structure built on a 22 × 30 × 8.6 mm poly-methyl methacrylate base containing a 1-mm-diameter round fluid inlet and outlet port. A polycarbonate track-etched membrane, or screen filter, with 0.4-μm pores (Isopore Millipore) and underlying support were embedded within the base, sealed with laminate adhesives containing a precision-cut fluid delivery channel and topped with a glass coverslip. Laminate cut-out structures were created using SolidWorks 3D CAD software and cut at 25-μm resolution using a Summa-Cut D-60 vinyl plotter cutter. Dimensions of the fluidic channel are 1 mm wide by 125 μm high by 8.2 mm long, generating a channel volume of 1.1 μL. The circular membrane capture area and imaging window is 5 mm wide by 200 μm high resulting in a reaction volume of 3.9 μL above the membrane surface. Fluid and sample delivery was facilitated by a peristaltic pump with a six-port injection valve at flow rates between 250 and 725 μL/min. Cells retained on the surface of the membrane using this straightforward filtration mechanism were analyzed for protein and/or nucleic acids using assay-specific fluorescent labeling techniques as described below. The efficiency of membrane capture is dependent on the ratio of particle size or, in this instance, cell size (typically 10 μm) to membrane pore size (0.4 μm). According to the manufacturer, >99% capture efficiency is obtained for particles exceeding the membrane pore size of 0.4 μm.

Sample collection and processing

Exfoliative cytology specimens were collected using the OralCDx cytology brush by placing the nylon brush firmly against the epithelial surface and rotating 10 to 15 times, while applying moderate pressure, until pinpoint bleeding was attained. Cells were then released from the biopsy brush and suspended in cold Eagle's MEM supplemented with 2 mmol/L L-glutamine and 10% fetal bovine serum using vigorous agitation for 15 to 30 s. Medium was removed by centrifugation at 1,200 rpm for 5 min. Cells were then washed twice in PBS buffer (BupH Modified Dulbecco's PBS Packs, Pierce/Thermo Fisher Scientific) by centrifugation at 1,200 rpm for 5 min. After the final wash, the supernatant was discarded and the cell pellet was resuspended in fetal bovine serum with 10% DMSO and frozen at −80°C for long-term storage and transport. In preparation for analysis, frozen samples were thawed rapidly in a 37°C water bath, washed twice in PBS, and fixed in 0.5% methanol-free formaldehyde (Polysciences, Inc.) in PBS buffer at 4°C for 20 min to 1 h. Following fixation, cells were washed twice in PBS and stored in PBS with 0.1% bovine serum albumin (PBSA) at 4°C for up to 1 wk. Healthy brush biopsy samples were all collected from the buccal mucosa, whereas clinical samples were collected from the lesion site or surgically excised tissue using similar protocols. When multifocal regions of irregularity were present, multiple brush biopsies from the same lesions were taken, sampling clinically distinct lesion areas.

Cell staining

Approximately 2,500 to 5,000 cells were suspended in 50% glycerol in PBSA, then delivered/captured on the NBC sensor membrane at a flow rate of 2 mL/min for 30 s followed by a 2.5-min PBS buffer wash at 1 mL/min. Next, fluorescent labeling was carried out through sequential delivery of immunoreagents, consisting of primary anti-EGFR antibody (LabVision) at 10 μg/mL in PBSA containing 0.1% Tween 20 (PBSAT) followed by a secondary antibody cocktail containing 20 μg/mL goat anti-mouse IgG/AlexaFluor-488 antibody fragment (Molecular Probes), 33 μmol/L phalloidin/AlexaFluor-647 (Molecular Probes), and 5 μmol/L 4′,6-diamidino-2-phenylindole (DAPI; Molecular Probes) in PBSAT. All reagents were delivered to the membrane-captured cells at 250 μL/min for 2.5 min with intermittent buffer washes at 1 mL/min for 2.5 min. Total assay time (without imaging and analysis) was 13 min.

Imaging and analysis

Digital micrographs of stained cells were obtained in an (*X*, *Y*, *Z*) membrane scan using a 10× (0.3 NA) objective on an automated Olympus BX-61 modified epifluorescent microscope with motorized stage and 12-bit monochrome charge-coupled device camera (Q-Imaging) controlled via Simple PCI software (Compix, Inc.). Monochrome images of phalloidin, EGFR, and DAPI fluorescent labels were collected sequentially using appropriate filter cubes (Chroma Technology Corp.) and then merged into red, green, and blue (RGB) spectral channels, respectively. Multiple *Z*-focal planes were collected at +5-μm intervals and recombined using a *z*-stack focusing algorithm in ImageJ (30) to accommodate adherent epithelial cell populations with both individual and aggregated cell clusters. Automated image analysis routines used ImageJ and/or Cell Profiler (31) open-source software with custom-written macros for quantitative intensity standardization and cell/nuclear contouring to define the region of interest (ROI) for each object/cell (27). Measurement parameters included whole cell and nuclear area, perimeter, circularity, Feret diameter, minimum and maximum intensity, mean, SD, mode, median, and integrated intensity. All together, 51 parameters, including 9 morphologic and 42 intensity parameters, were extracted or calculated for each cell with an average of 1,420 cells measured in each cytology sample (range, 50-3,624). For statistical analysis, data were exported to Microsoft EXCEL with Analyse-It (Analyse-It Software Ltd.) software and SigmaPlot 9.0 (Systat Software, Inc.) for graphical representation.

Study participants and demographics

A total of 52 participants were enrolled in this study from May 2007 to March 2009. Eleven of these volunteers were healthy individuals with no known oral diseases or signs of epithelial abnormality within the oral cavity. An additional 41 clinical participants were identified by collaborating dentists and physicians located at the University of Texas Health Science Center (UTHSC) at San Antonio ($n = 22$) and Houston ($n = 19$). Eligibility criteria included patients presenting with a visible oral lesion(s), leukoplakia, or erythroplakia, who were referred to specialists in secondary or tertiary care centers for surgical biopsy or removal. Informed consent was obtained from all participants and the study guidelines were approved by the Institutional Review Board at each institution.

The demographic data and pathologic diagnosis available from clinical participants are provided in Table 1. Of the 41 clinical cases, 66% were male, 85% had a history of tobacco use, and 42% also reported moderate to heavy alcohol consumption. The average age in this clinical group was 56 years (range, 31-79 years) and the majority of lesions occurred in the tongue or floor of the mouth. Diagnosis was established for each patient by surgical biopsy of the lesion site and standard histopathology by board-certified oral and maxillofacial pathologists at their respective institutions. The group of 11 healthy participants consisted of 55% males with an average age of 33 years (range, 21-53 y). Only one of the healthy participants reported a history of smoking.

Statistical analysis

A Student's *t* test (Analyze-It for MS Excel) was used to assess statistically significant differences in the measured cellular parameters within each study group, including benign lesions, dysplasia, and invasive squamous cell carcinoma (SCC), when compared with the healthy controls

Table 1. Demographic data and pathologic diagnosis for study participants enrolled at UTHSC San Antonio and Houston clinics

Patient ID	Age (y)	Sex	Lesion location	Pathologic diagnosis
UTSA-001	48	M	Floor of mouth	SCC, moderately differentiated
UTSA-002	56	M	Tongue, base	SCC, poorly differentiated
UTSA-003	57	M	Soft palate	Dysplasia, mild-moderate
UTSA-004	44	M	Soft palate and tonsil	SCC, moderately differentiated
UTSA-005	40	M	Tongue, lateral	SCC
UTSA-006	48	M	Hard palate	Benign hyperkeratosis and oral submucous fibrosis
UTSA-007	45	F	Tongue, ventral	SCC
UTSA-008*	44	M	Alveolar ridge	Lymphoma
UTSA-009	64	M	Retromolar trigone	SCC
UTSA-010	59	M	Tongue, ventrolateral	SCC, well differentiated
UTSA-011	62	M	Soft palate	SCC, moderately differentiated
UTSA-012	60	M	Tongue, lateral	SCC, moderately differentiated
UTSA-013	42	F	Tongue, lateral	SCC, moderate to poorly differentiated
UTSA-014	59	F	Floor of mouth/tongue	SCC, moderately differentiated
UTSA-015	64	M	Palate	SCC, moderately differentiated
UTSA-016	72	F	Hard palate	SCC, well to moderately differentiated
UTSA-017	68	M	Hard palate	SCC, verrucous carcinoma
UTSA-018	50	F	Soft palate	SCC, poorly differentiated
UTSA-019	70	F	Pharynx	SCC
UTSA-020	30	M	Tongue, lateral	SCC, well differentiated
UTSA-021	48	M	Tongue/floor of mouth	SCC, moderately differentiated
UTSA-022	55	M	Retromolar trigone	SCC, moderately differentiated
UTH-001	56	M	Hard palate	SCC, moderately differentiated
UTH-002	68	M	Hard palate	SCC, moderately differentiated
UTH-003	53	M	Tongue	SCC, moderately differentiated
UTH-004	52	M	Tongue/floor of mouth	SCC, moderately differentiated
UTH-005	74	F	Tongue	SCC, residual ulcerated
UTH-006	47	M	Tongue/floor of mouth	SCC, moderately differentiated
UTH-007	75	F	Tongue	Dysplasia, moderate
UTH-008	50	M	Tongue	SCC, moderately differentiated
UTH-009	79	F	Tongue	SCC, moderately differentiated
UTH-010	69	M	Tongue	SCC, moderately differentiated, superficially invasive
UTH-011	62	F	Gingiva	Dysplasia, severe
UTH-012	51	F	Palate	Benign lichen planus
UTH-013	31	M	Tongue, lateral	Dysplasia, moderate
UTH-014	60	M	Tongue, ventral	Dysplasia, moderate
UTH-015	65	F	Tongue/floor of mouth	Dysplasia, moderate
UTH-016	41	M	Buccal mucosa	Dysplasia, mild with submucosal fibrosis
UTH-017	52	F	Tongue, lateral	Dysplasia, moderate-severe
UTH-018	72	M	Tongue	SCC, verrucous carcinoma
UTH-019	60	F	Soft palate	Dysplasia, moderate in atypical verrucous/papillary hyperplasia

*Patient was excluded from the study due to nonepithelial nature of malignancy.

($P < 0.05$). Logistic regression and receiver operating characteristic (ROC) curve analyses were done using MedCalc (MedCalc Software) statistical software. This method requires the input of parameter values measured for each sample (i.e., EGFR intensity, nuclear and cellular area, etc.) according to a binary classification of disease status where nondiseased samples received a value of zero and diseased samples, one (nondiseased, 0; diseased, 1). The logistic function, with the general equation of $f(z) = 1/[1 + \exp(-z)]$, serves to predict the probability of an outcome (disease occurrence) between 0 and 1 based on one or more of these input parameters or factors. The variable z is a measure of the total contribution of all the factors used in the model, according to the logit equation $z = a_0$

+ $a_1 \times BM_1 + a_2 \times BM_2 + \ldots, a_n \times BM_n$, where a_0 is the intercept and $a_1 \ldots, a_n$ are the regression coefficients for each biomarker ($BM_1 \ldots, BM_n$). Predicted values using the linear regression model were used to build ROC curves plotting the projected true-positive and false-positive rates (sensitivity versus 1 – specificity) for disease classification based on the model.

Results

As illustrated in Fig. 1, the NBC sensor system for OSCC assessment integrates multiple laboratory processes into a microfluidic platform in three primary steps consisting of (*a*) cell separation/capture on the membrane filter, (*b*) biomarker immunolabeling and cytochemical staining,

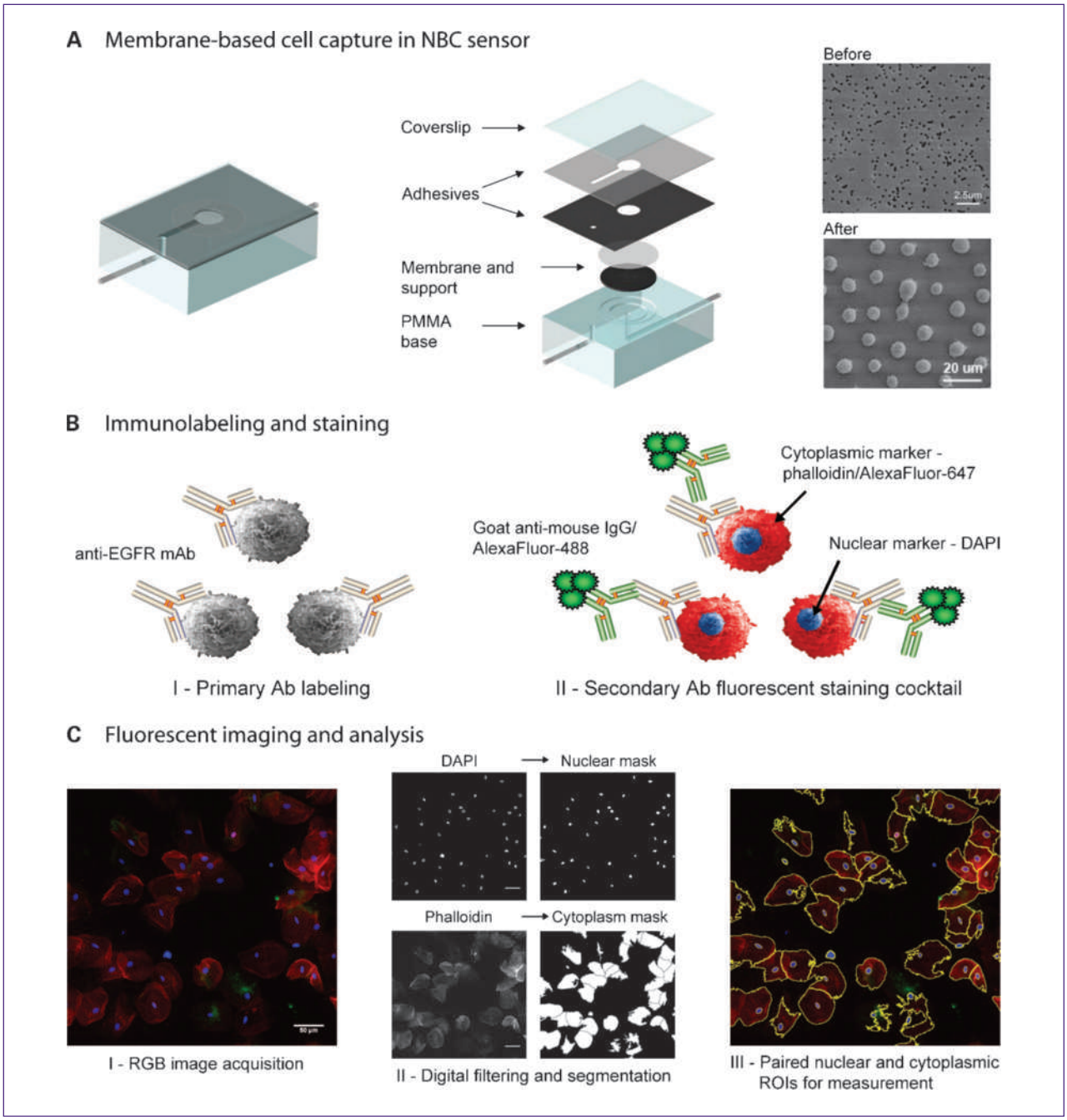

Fig. 1. The NBC oral cytology assay consists of three primary steps: (A) cell capture on the membrane filter; (B) EGFR/AlexaFluor-488 immunolabeling and staining with phalloidin/AlexaFluor-647 and DAPI; and (C) fluorescent imaging and analysis, where paired cytoplasmic/nuclear ROIs are defined for each cell.

Table 2. Results of NBC sensor analysis of EGFR biomarker expression and cytomorphometry in oral lesions according to histopathologic diagnosis

	Healthy (n = 11)	Benign (n = 3)	Dysplasia (n = 7)	SCC (n = 31)
Nuclear area (μm^2)	63.4 ± 11	122 ± 57*	149 ± 23*	165 ± 46*
		$P < 0.004$	$P < 0.001$	$P < 0.001$
Nuclear diameter (μm)	11.5 ± 0.70	14.8 ± 3.2*	16.1 ± 1.2*	17.3 ± 2.6*
		$P < 0.005$	$P < 0.001$	$P < 0.001$
Cellular area (μm^2)	1,040 ± 160	1,300 ± 500	1,040 ± 260	697 ± 230*
		$P < 0.15$	$P < 0.99$	$P < 0.001$
Cellular diameter (μm)	51.5 ± 4.4	55.1 ± 12	49.9 ± 6.3	41.1 ± 7.1*
		$P < 0.4$	$P < 0.6$	$P < 0.001$
N/C ratio	0.063 ± 0.02	0.206 ± 0.17*	0.223 ± 0.10*	0.323 ± 0.14*
		$P < 0.01$	$P < 0.001$	$P < 0.001$
EGFR intensity (au)	5.99 ± 1.4	7.10 ± 1.8	9.53 ± 4.3*	11.8 ± 6.5*
		$P < 0.3$	$P < 0.03$	$P < 0.006$

NOTE: Data are presented as mean ± SD.
*Statistically significant difference relative to healthy controls using paired t test ($P < 0.05$).

and (*c*) fluorescent imaging and analysis. During cell capture, an oral cytology suspension is delivered to the NBC sensor, using pressure-driven flow, whereupon any particles or cells larger than the membrane pore size are retained on the membrane surface (Fig. 1A). Once captured, a series of biomarker-specific immunoreagents and cellular stains (Fig. 1B, I and II, respectively) are used to tag the epithelial cells of interest, which are then detected using fluorescence microscopy in an *X*, *Y*, *Z* scan of the membrane surface (Fig. 1C, I). Subsequent automated image analysis routines use digital filtering and image segmentation of the DAPI and phalloidin signals, blue and red spectral channels, respectively, to generate binary masks and contours of the nuclear and cytoplasmic ROIs for measurement in all fluorescent channels (Fig. 1C, II and III). This semiautomated NBC methodology permits concurrent analysis of EGFR surface biomarker expression and cellular/nuclear morphology using more than 50 ROI intensity and shape parameters, with particular attention focused on the cellular and nuclear area, the nuclear-to-cytoplasmic (N/C) ratio, and mean cellular EGFR intensity as early indicators of malignancy.

Cytomorphometry and EGFR biomarker expression analysis

A total of 56 oral brush cytology specimens from healthy and disease participants were examined using the NBC sensor method. Eleven specimens were obtained from healthy individuals and 45 were from clinically visible lesions identified in 41 patients (Table 1). Histopathologic diagnosis identified 3 benign lesions, 8 moderate or severely dysplastic lesions, and 34 invasive SCCs (Table 1). Two of the SCC samples were expended during the initial assay development stages, whereas another SCC and one dysplasia specimen were excluded due to inadequate cell sampling for a sampling error rate of ~4%.

Table 2 summarizes the NBC sensor results obtained from the remaining 52 brush cytology specimens analyzed for cytomorphometry and EGFR biomarker expression. Here, the nuclear area was significantly increased in dysplastic and invasive SCC cytospecimens (149 and 165 μm^2, respectively) versus healthy control epithelium (63.4 μm^2; $P < 0.0001$). Similarly, the nuclear diameter was also elevated in dysplastic and SCC lesions (16.1 and 17.3 μm, respectively) relative to healthy mucosa (11.5 μm; $P < 0.0001$). Concurrent with this nuclear enlargement was a decrease in the cellular area from 1,040 μm^2 in healthy mucosa to 697 μm^2 in SCC ($P < 0.0001$), as well as a decrease in cellular diameter from 51.5 μm in healthy specimens to 41.1 μm in SCC ($P < 0.001$). This inverse relationship, with an overall increase in nuclear size and a decrease in cellular size, yielded a significant elevation in the N/C ratio. Interestingly, this increase in the N/C ratio seemed to be progressive from healthy mucosa (0.063) through precancerous lesions with moderate and/or severe dysplasia (0.223; $P < 0.0001$) to invasive SCC (0.323; $P < 0.001$) although the difference in N/C ratio between dysplastic and SCC lesions was not significant ($P < 0.08$). The EGFR labeling intensity was also shown to increase significantly in diagnosed dysplasia and OSCC relative to healthy epithelium (9.5, 11.8, and 6.0 au, respectively; Table 2). Cytology specimens from the three benign lesions exhibited an increase in nuclear area/diameter and N/C ratio over controls ($P < 0.005$), but their EGFR intensity remained similar to normal oral mucosa. There were no statistically significant differences between patient samples collected at UTHSC San Antonio and Houston facilities for any of the parameters measured (data not shown).

Further examination of the population distribution within individual samples revealed additional features that could potentially be exploited for disease characterization. Box and whisker plots presented in Fig. 2 depict the median, interquartile range, and outliers of nuclear area measurements from a subset of patients. Here, the median nuclear area for healthy control specimens ranged from 47 to 63 μm^2, whereas the SCC and dysplasia samples exhibited median values from 66 to 141 μm^2. Interestingly, it is the spread of outliers that seemed to be the most distinguishing characteristic from which to differentiate normal cytology specimens from dysplasia and invasive SCC. As such, none of the healthy specimens possess outliers >500 μm^2, whereas all of the SCC/dysplasia possessed numerous events above this level.

Case study: comparison with histology and immunohistochemistry

Whereas histology and EGFR immunohistochemistry were done for all surgically biopsied oral tissues, two cases were selected to show the similarities and difference in the type and range of cellular features examined in traditional diagnostic methods versus the NBC sensor system using brush cytology (Fig. 3). One case was diagnosed as mild to moderate dysplasia in the soft palate (Fig. 3A) and the other an invasive squamous cell carcinoma located on the ventral tongue (Fig. 3E). In the H&E-stained tissue shown in Fig. 3A, a thin keratin layer is seen at the surface of the epithelium with the various stratified layers beneath, relatively normal for mucosa at this oral cavity site. On higher magnification (Fig. 3B), several dysplastic features are seen including enlarged and pleomorphic nuclei found above the basal cell layer, with loss of basal cell polarity and maturation sequence. Corresponding EGFR immunohistochemistry revealed EGFR (+) positive membrane labeling in the lower layers of the epithelium, including the basal cells, which dissipated in the more superficial layers and in the surface epithelium (Fig. 3C). Cytologic analysis using the NBC sensor assay from this patient displayed a heterogeneous mixture of EGFR-positive (+) and EGFR-negative (–) labeled epithelial cells (Fig. 3D), derived from the differential EGFR-expressing epithelial layers as depicted in immunohistochemistry, along with an elevated nuclear area (~120 μm^2). This pattern suggests that the NBC cytologic method may effectively reflect biochemical and morphologic changes in neoplastic tissue, even at these early premalignant stages.

Similar pathologic features were also seen in the OSCC tissue, albeit more pronounced, with dyskeratosis, cellular and nuclear pleomorphism, and mitotic figures visible in H&E-stained sections (Fig. 3E and F), whereas immunohistochemistry showed strong EGFR (+) labeling throughout the tumor (Fig. 3G). In the NBC sensor cytology assay, extremely intense EGFR (+) labeling was also detected and localized in the cell membranes of adherent epithelial cell clusters as well as some individual cells (Fig. 3H, inset). In the particular cluster shown, a number of the nuclei present also appear irregular and/or enlarged, indicating that these cells exhibit "cancer-like" nuclear characteristics reflective of what is seen in tumor tissue.

ROC curve analysis and logistic regression

Logistic regression and ROC curve analyses enabled further exploration into which of these cellular markers, and in what combinations, could be most effective toward diagnosis of OSCC. Each individual parameter was

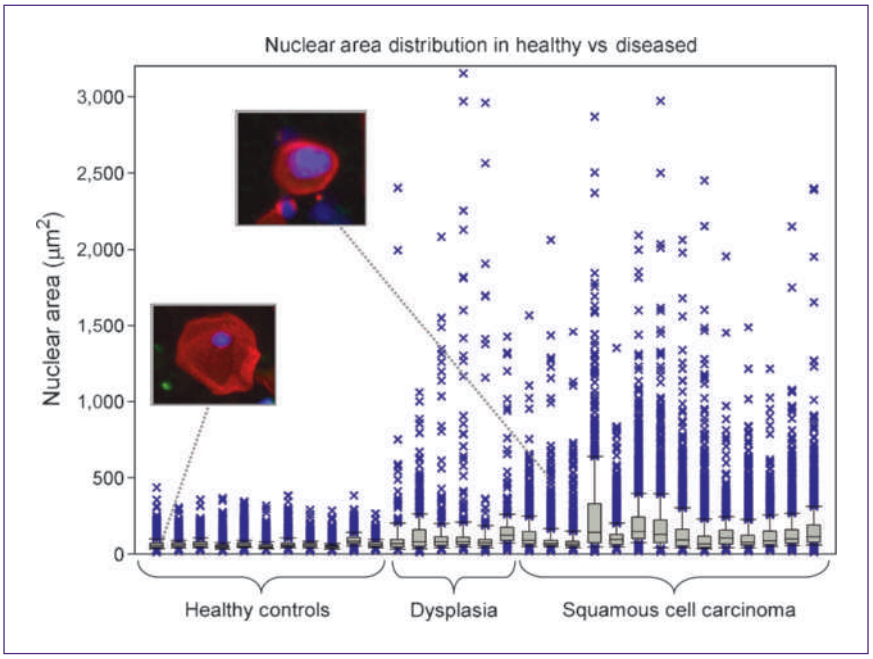

Fig. 2. Box and whisker plot of the median, interquartile range, and the distribution of outliers in the nuclear area data for each cell population according to disease status. Two representative cells from a healthy participant and SCC patient are shown (inset).

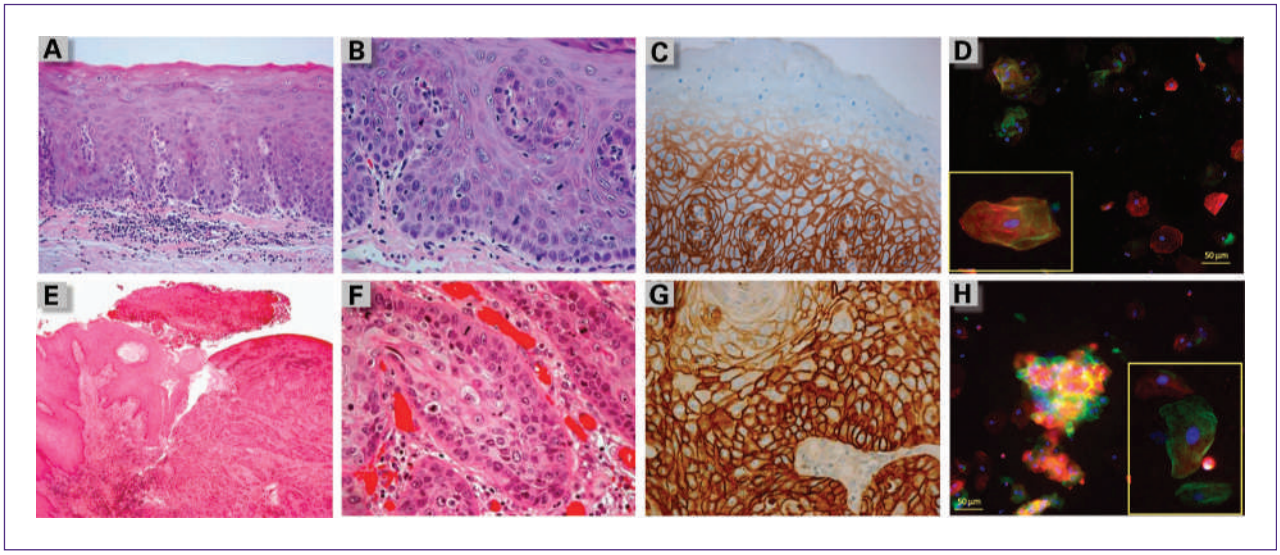

Fig. 3. Comparison of histology, immunohistochemistry, and NBC sensor micrographs in case studies of mild to moderate dysplasia (A-D) and invasive SCC (E-H). H&E sections at low magnification (A and E) show the overall tissue architecture, whereas at higher magnification (B and F), abnormal cellular alterations, such as nuclear enlargement, loss of polarity, and an increase in the number mitotic figures, are visible. EGFR immunohistochemistry using peroxidase-3,3′-diaminobenzidine staining (C and G) identifies the differential expression of EGFR within the dysplastic/malignant tissue. Micrographs from NBC sensor assay (D and H) show a corresponding heterogeneous mixture of normal and "abnormal" cells with elevated EGFR biomarker expression and enlarged nuclei (inset).

evaluated by a ROC curve, as shown in Fig. 4A to C for EGFR, N/C ratio, and nuclear area. The ROC curve is a plot of diagnostic test sensitivity, or true-positive rate versus 1 – specificity, or the false-positive rate at various discrimination thresholds depicting the trade-offs between the true positives (benefits) and the false positives (costs) in diagnostic accuracy. All of the parameters tested exhibited significant capacity for disease classification and discrimination between patients with OSCC or dysplasia and healthy controls or benign conditions, as shown by the area under the curve (AUC) values >0.5. Of these parameters, the N/C ratio and nuclear area exhibited the best performance characteristics with AUC of 0.93, followed by the EGFR biomarker (0.82; Fig. 4A-C). The N/C ratio or nuclear areas, alone, are excellent diagnostic markers, and the added value of these markers in a combined panel was further examined using logistic regression. Here, the ROC curve generated from the predicted values in the combined biomarker panel exhibited AUC of 0.94 with a projected 97% sensitivity and 93% specificity for detection and classification of malignant and premalignant oral lesions (Fig. 4D).

Discussion

In this pilot study, a new NBC cellular analysis technique for characterizing oral malignant and premalignant lesions was evaluated. Six parameters were found to be significantly altered in OSCC cytospecimens versus healthy mucosa, including (*a*) nuclear area, (*b*) nuclear diameter, (*c*) cellular area, (*d*) cellular diameter, (*e*) nuclear-to-cytoplasmic ratio, and (*f*) EGFR biomarker immunolabeling (Table 2). The nuclear area, nuclear diameter, N/C ratio, and EGFR expression were also found to be significantly altered in oral lesions with diagnosed dysplasia, supporting the use of these markers as diagnostic indicators of early cancer development and premalignancy. These findings are in line with earlier reports by Ramesh et al. and Grandis et al. identifying significant changes in cellular and nuclear morphology and EGFR expression associated with oral tumorigenesis (32–34), while providing a new method for automated cytoanalysis that is rapid, quantitative, and requires small sample volumes. Using the mean EGFR intensity values from healthy control subjects (Table 2) plus 2 SD (6.0 ± 2.8), a rough threshold for EGFR overexpression can be established. According to this criterion, 63% (20 of 32) of SCC tumors and 67% (4 of 6) of precancerous dysplastic lesions overexpress the EGFR biomarker, whereas none (0 of 3) of the benign specimens exhibit biomarker overexpression. Interestingly, these benign lesions showed a significantly elevated nuclear area and N/C ratio, but not EGFR expression, relative to normal controls (Table 2). Although the number of benign oral lesions examined in this study is small, this finding suggests that both morphologic and biochemical markers are important for successful characterization of oral lesions, particularly when discriminating them from other nonmalignant conditions and inflammation (35). This issue will be explored more thoroughly in future studies.

In addition to the mean values, we examined the population distribution, with particular attention toward outliers in the data. These outliers likely represent the "rare events" important for early disease detection, which may be obscured or masked in mean measurements over the

entire population. As shown in Fig. 2, the spread of outliers in the nuclear area measurements visibly distinguishes healthy controls from dysplasia and SCC. Particularly for dysplastic lesions, this makes sense, where the top of the mucosa is mature and pathologically similar to healthy normal epithelium, whereas it is the smaller portion of deep cells that contain the information about the presence and extent of abnormality. As such, many of the cells in a cytology suspension would be expected to possess N/C ratios in the reference range and only a fraction of the cells would be expected to exhibit dysplastic/malignant changes (i.e., an elevation in the N/C ratio, represented here as the N/C ratio outliers). A new calculated parameter, such as a "polymorphic index," representing the range in this distribution or ratio of identifiable cell types may provide an addition handle from which to classify disease with enhanced accuracy over mean values in future assays.

Comparison of the NBC cellular analysis methods with standard histopathology and immunohistochemistry, as shown in Fig. 3, offers insight into the types of malignant features available with each method and their associated benefits and trade-offs. Based on standard histopathology, case one was diagnosed with mild to moderate dysplasia and exhibits several abnormal/enlarged nuclei along with a loss of basal cell polarity in H&E-stained tissue sections, but with the overall epithelial structure and stratification maintained (Fig. 3A and B). The immunohistochemistry revealed EGFR expression restricted to the lower layers of epithelium (Fig. 3C). These alterations in nuclear morphology and EGFR expression were successfully detected and quantitated in the NBC sensor assay (Fig. 3D), suggesting that the sensor method adequately reflects cellular alterations in tumor tissue, even at early premalignant stages. A similar comparison was seen in the case of invasive SCC (Fig. 3E-H) where intense EGFR staining was apparent throughout the epithelium in immunohistochemically stained histologic sections as well as in a cluster of "cancer-like" cells with EGFR (+) membrane labeling and enlarged nuclei in the NBC sensor (Fig. 3H, inset). When using the bio-chip sensor system, a trade-off exists between the loss of information on cellular architecture and cell-cell or cell-matrix interactions and the added benefit of a rapid, noninvasive automated cellular analysis technique.

Evaluation of which cellular and biochemical markers, alone or in combination, could be most effective toward diagnosis of malignant and premalignant oral lesions was undertaken in a more quantitative manner using logistic regression and ROC curves analyses (Fig. 4). Logistic

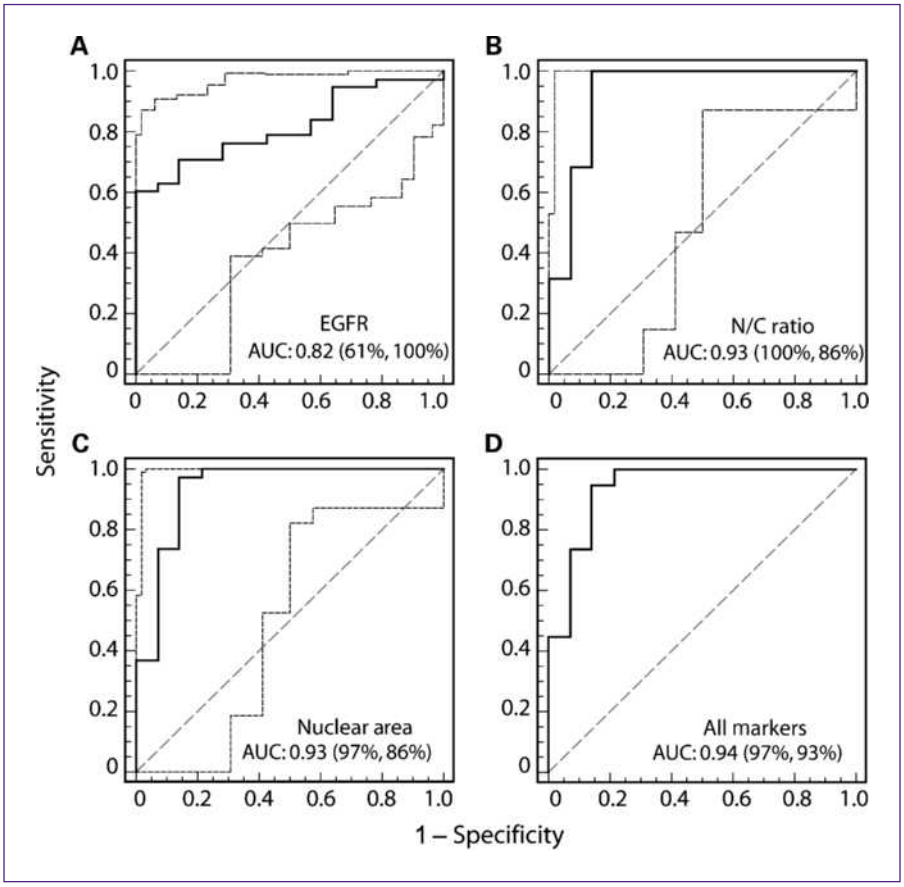

Fig. 4. ROC curves for evaluation of the diagnostic performance characteristics for the individual markers: EGFR (A), N/C ratio (B), and nuclear area (C). Using a logistic regression model, the combined EGFR and cytomorphometry marker panel (D) is predicted to exhibit an AUC value of 0.94 with 97% sensitivity and 93% specificity for characterization of oral malignant and premalignant lesions.

regression serves as a model to predict the outcome of disease, based on input of one or more variables, such as the N/C ratio, nuclear area, and EGFR biomarker measurements obtained in NBC sensor assays. The predicted values generated from logistic regression were used to build ROC curves, a graphical representation of diagnostic test sensitivity, or true-positive rate versus 1 – specificity, or the false-positive rate at various discrimination thresholds. In Fig. 4, the ROC curves for the EGFR biomarker, nuclear area, and N/C ratio are presented for the combined patient population. Here, the EGFR biomarker exhibited moderate disease discrimination capability with an AUC value of 0.82, whereas the nuclear area and N/C ratio both exhibited AUC values of 0.93, indicating excellent disease classification performance. The logistic regression model and ROC curve for a three-marker panel (Fig. 4D) exhibited a slight increase in AUC value to 0.94 with a predicted sensitivity of 97% and a specificity of 93%. These results suggest that the combined cytomorphometry and EGFR panel likely holds the greatest potential for cancer detection and diagnosis. Yet, the true diagnostic need lies not in the identification of oral cancer but in the identification of premalignant lesions. Analysis of the data from Fig. 4 that includes dysplasia only (moderate or severe) yielded AUC values of 0.83 for EGFR, 0.90 for the N/C ratio, and 0.92 for the nuclear area (data not shown). Unfortunately, the limited number of dysplastic samples prevented further statistical analysis using logistic regression, which typically requires a minimum of 10 cases per independent variable (36). However, the close similarity between AUC values from dysplasia alone and the combined patient population suggests that the parameters that were most predictive in the combined cohort are also predictive of oral premalignancy.

It is important to note that this work represents a development effort for a novel NBC system with integrated microfluidic elements and proof-of-principle study, not a validation of a commercial product. As such, the clinical implications are somewhat limited due to a relatively small sample size, particularly within the benign and dysplasia diagnostic categories, and an uneven distribution of samples between the diagnostic groups that can weigh one category too heavily in comparative analyses. In particular, the SCC group accounted for 60% of all samples. Such imbalances are often found in early-stage diagnostic development studies where clinical collaborators are typically located in regional specialty clinics or research-based cancer centers where the patient population is skewed toward more severe cases of dysplasia and/or SCC (37, 38).

However, the largest challenge for early detection in the oral cavity is not the diagnosis of actual SCC, rather it is determining which "innocuous" lesions may be biologically worrisome. Building on the promising cytoanalysis techniques presented here, our future research studies target a cohort of ~850 patients presenting with oral leukoplakia, or otherwise "innocuous" lesions, which may harbor early signs of dysplasia and molecular transformation. These prospective studies will target a low-risk population and greatly expand the sample size to improve the statistical power of NBC sensor results. In addition, we will examine the role of benign inflammation in assay specificity while continuing to integrate and evaluate additional disease-specific biomarkers. We believe that the true potential for this work rests in the ability to extend the rapid assay techniques developed here for examination of multiple disease-specific biomarkers in an effort to improve risk assessment and early detection and the specificity of oral diagnostics.

Disclosure of Potential Conflicts of Interest

J.T. McDevitt: ownership interest and consultant/advisory board, LabNow. The other authors disclosed no potential conflicts of interest.

Acknowledgments

We thank Dr. Rebecca Richard-Kortum at Rice University for her generous assistance and insight throughout this research.

Grant Support

Funding for this work was provided by the National Institutes of Health (NIH) through the National Institute of Dental and Craniofacial Research (1RC2DE020785 and 1U01DE017793). The content is solely the responsibility of the authors and does not necessarily represent or reflect views of the NIH or the U.S. government.

The costs of publication of this article were defrayed in part by the payment of page charges. This article must therefore be hereby marked *advertisement* in accordance with 18 U.S.C. Section 1734 solely to indicate this fact.

Received 06/30/2009; revised 11/30/2009; accepted 12/16/2009; published OnlineFirst 03/23/2010.

References

1. Parkin DM, Bray F, Ferlay J, Pisani P. Global cancer statistics, 2002. CA Cancer J Clin 2005;55:74–108.
2. American Cancer Society. Cancer facts and figures. Atlanta (GA): American Cancer Society; 2008.
3. Seiwert TY, Cohen EE. State-of-the-art management of locally advanced head and neck cancer. Br J Cancer 2005;92:1341–8.
4. Ries LAG MD, Krapcho M, Mariotto A, et al. SEER cancer statistics review 1975-2004. Bethesda (MD): National Cancer Institute.
5. Lee JJ, Hong WK, Hittelman WN, et al. Predicting cancer development in oral leukoplakia: ten years of translational research. Clin Cancer Res 2000;6:1702–10.
6. Schepman KP, van der Meij EH, Smeele LE, van der Waal I. Malignant transformation of oral leukoplakia: a follow-up study of a hospital-based population of 166 patients with oral leukoplakia from the Netherlands. Oral Oncol 1998;34:270–5.
7. Speight PM, Farthing PM, Bouquot JE. The pathology of oral cancer and precancer. Curr Diag Pathol 1996;3:165–76.
8. Reibel J. Prognosis of oral pre-malignant lesions: significance of clinical, histopathological, and molecular biological characteristics. Crit Rev Oral Biol Med 2003;14:47–62.
9. van der Waal I, Schepman KP, van der Meij EH, Smeele LE. Oral leukoplakia: a clinicopathological review. Oral Oncol 1997;33:291–301.
10. Karabulut A, Reibel J, Therkildsen MH, Praetorius F, Nielsen HW, Dabelsteen E. Observer variability in the histologic assessment of oral premalignant lesions. J Oral Pathol Med 1995;24:198–200.
11. Abbey LM, Kaugars GE, Gunsolley JC, et al. Intraexaminer and

interexaminer reliability in the diagnosis of oral epithelial dysplasia. Oral Surg Oral Med Oral Pathol Oral Radiol Endod 1995;80:188–91.
12. Sugerman PB, Savage NW. Exfoliative cytology in clinical oral pathology. Aust Dent J 1996;41:71–4.
13. Ogden GR, Cowpe JG, Green M. Cytobrush and wooden spatula for oral exfoliative cytology. A comparison. Acta Cytol 1992;36: 706–10.
14. Ogden GR. The future role for oral exfoliative cytology—bleak or bright? Oral Oncol 1997;33:2–4.
15. Driemel O, Dahse R, Hakim SG, et al. Laminin-5 immunocytochemistry: a new tool for identifying dysplastic cells in oral brush biopsies. Cytopathology 2007;18:348–55.
16. Spafford MF, Koch WM, Reed AL, et al. Detection of head and neck squamous cell carcinoma among exfoliated oral mucosal cells by microsatellite analysis. Clin Cancer Res 2001;7:607–12.
17. Schwartz JL, Panda S, Beam C, Bach LE, Adami GR. RNA from brush oral cytology to measure squamous cell carcinoma gene expression. J Oral Pathol Med 2008;37:70–7.
18. Veltman JA, Hopman AH, Bot FJ, Ramaekers FC, Manni JJ. Detection of chromosomal aberrations in cytologic brush specimens from head and neck squamous cell carcinoma. Cancer 1997;81: 309–14.
19. Sciubba JJ, U.S. Collaborative OralCDx Study Group. Improving detection of precancerous and cancerous oral lesions. Computer-assisted analysis of the oral brush biopsy. J Am Dent Assoc 1999; 130:1445–57.
20. Lingen MW, Kalmar JR, Karrison T, Speight PM. Critical evaluation of diagnostic aids for the detection of oral cancer. Oral Oncol 2008; 44:10–22.
21. Poate TW, Buchanan JA, Hodgson TA, et al. An audit of the efficacy of the oral brush biopsy technique in a specialist Oral Medicine unit. Oral Oncol 2004;40:829–34.
22. Scheifele C, Schmidt-Westhausen AM, Dietrich T, Reichart PA. The sensitivity and specificity of the OralCDx technique: evaluation of 103 cases. Oral Oncol 2004;40:824–8.
23. Ali MF, Kirby R, Goodey AP, et al. DNA hybridization and discrimination of single-nucleotide mismatches using chip-based microbead arrays. Anal Chem 2003;75:4732–9.
24. Christodoulides N, Floriano PN, Miller CS, et al. Lab-on-a-chip methods for point-of-care measurements of salivary biomarkers of periodontitis. Oral-Based Diagnostics 2007:411–28.
25. Rodriguez WR, Christodoulides N, Floriano PN, et al. A microchip CD4 counting method for HIV monitoring in resource-poor settings. Plos Medicine 2005;2:663–72.
26. Floriano PN, Christodoulides N, Romanovicz DK, et al. Membrane-based on-line optical analysis system for rapid detection of bacteria and spores. Biosens Bioelectron 2005;20:2079–88.
27. Weigum SE, Floriano PN, Christodoulides N, McDevitt JT. Cell-based sensor for analysis of EGFR biomarker expression in oral cancer. Lab Chip 2007;7:995–1003.
28. Grandis JR, Tweardy DJ. Elevated levels of transforming growth factor α and epidermal growth factor receptor messenger RNA are early markers of carcinogenesis in head and neck cancer. Cancer Res 1993;53:3579–84.
29. Shin DM, Ro JY, Hong WK, Hittelman WN. Dysregulation of epidermal growth factor receptor expression in premalignant lesions during head and neck tumorigenesis. Cancer Res 1994;54:3153–9.
30. Rasband WS. Image J. Bethesda (MD): U.S. National Institutes of Health; 19997–2006.
31. Carpenter AE, Jones TR, Lamprecht MR, et al. CellProfiler: image analysis software for identifying and quantifying cell phenotypes. Genome Biol 2006;7:R100.
32. Pektas ZO, Keskin A, Gunhan O, Karslioglu Y. Evaluation of nuclear morphometry and DNA ploidy status for detection of malignant and premalignant oral lesions: quantitative cytologic assessment and review of methods for cytomorphometric measurements. J Oral Maxillofac Surg 2006;64:628–35.
33. Ramaesh T, Mendis BR, Ratnatunga N, Thattil RO. Cytomorphometric analysis of squames obtained from normal oral mucosa and lesions of oral leukoplakia and squamous cell carcinoma. J Oral Pathol Med 1998;27:83–6.
34. Cowpe JG, Longmore RB, Green MW. Quantitative exfoliative cytology of abnormal oral mucosal smears. J R Soc Med 1988;81:509–13.
35. Anuradha C, Reddy BV, Nandan SR, Kumar SR. Oral lichen planus. A review. N Y State Dent J 2008;74:66–8.
36. Peduzzi P, Concato J, Kemper E, Holford TR, Feinstein AR. A simulation study of the number of events per variable in logistic regression analysis. J Clin Epidemiol 1996;49:1373–9.
37. Lane PM, Gilhuly T, Whitehead P, et al. Simple device for the direct visualization of oral-cavity tissue fluorescence. J Biomed Opt 2006; 11:024006.
38. Ram S, Siar CH. Chemiluminescence as a diagnostic aid in the detection of oral cancer and potentially malignant epithelial lesions. Int J Oral Maxillofac Surg 2005;34:521–7.